# Mott versus Hybridization Gap in the Low-Temperature Phase of 1$T$-$TaS_2$

Francesco Petocchi,[1] Christopher W. Nicholson,[1,2] Bjoern Salzmann,[1] Diego Pasquier,[3] Oleg V. Yazyev,[3] Claude Monney,[1] and Philipp Werner[1]

[1]*Department of Physics, University of Fribourg, 1700 Fribourg, Switzerland*

[2]*Fritz-Haber-Institute der Max-Planck-Gesellschaft, Faradayweg 4-6, 14195 Berlin, Germany*

[3]*Institute of Physics, Ecole Polytechnique Fédérale de Lausanne (EPFL), 1015 Lausanne, Switzerland*

(Received 3 February 2022; revised 7 April 2022; accepted 1 June 2022; published 30 June 2022)

We address the long-standing problem of the ground state of 1$T$-$TaS_2$ by computing the correlated electronic structure of stacked bilayers using the $GW$ + EDMFT method. Depending on the surface termination, the semi-infinite uncorrelated system is either band insulating or exhibits a metallic surface state. For realistic values of the on-site and inter-site interactions, a Mott gap opens in the surface state, but it is smaller than the gap originating from the bilayer structure. Our results are consistent with recent scanning tunneling spectroscopy measurements for different terminating layers, and with our own photoemission measurements, which indicate the coexistence of spatial regions with different gaps in the electronic spectrum. By comparison to exact diagonalization data, we clarify the interplay between Mott insulating and band insulating behavior in this archetypal layered system.

DOI: 10.1103/PhysRevLett.129.016402

*Introduction.*—The layered transition metal dichalcogenide 1$T$-$TaS_2$ has been studied intensively for decades, because it exhibits an intriguing interplay between lattice distortions and correlated electron phenomena. The material undergoes a series of charge density wave (CDW) transitions as temperature is lowered, first to an incommensurate CDW phase at 550 K, then to a nearly commensurate CDW phase around 350 K, and below 180 K to a commensurate CDW (CCDW) phase [1]. An in-plane periodic lattice distortion in the CCDW state results in a triangular lattice of star-of-David (SOD) clusters consisting of 13 Ta atoms, and the resistivity strongly increases. Since 12 molecular orbitals of the SOD clusters are either filled or empty and one is half filled, the monolayer system can be described by a half-filled Hubbard model on a triangular lattice, which due to the narrow bandwidth becomes Mott insulating. Based on this picture, bulk 1$T$-$TaS_2$ in the CCDW state is often regarded as a polaronic Mott insulator [2]. Interesting properties of this phase include a transition to a superconducting state under pressure [3], and possible spin-liquid behavior [4]. It has also been shown that the CCDW phase can be switched into long-lived metallic metastable phases by the application of short laser or voltage pulses [5,6], which may be exploited in future memory devices [7]. The study of the equilibrium [6,8–10] and nonequilibrium [11] phases of 1$T$-$TaS_2$ by scanning tunneling microscopy (STM) have furthermore revealed nontrivial patterns and spatial regions with different gaps in the electronic spectrum.

On the theory side, the electronic structure of the CCDW phase has been studied in several recent works [9,12–16], and the Mott insulator picture has been challenged. Based on density functional theory (DFT) + $U$ calculations Ref. [12] argued that the system is Mott insulating in the in-plane direction, but, due to a strong hybridization between planes of vertically aligned SOD clusters, a widely dispersing metallic band is present in the stacking direction. Initial attempts to explain the insulating nature of the CCDW phase focused on stacking disorder, an effect that has long been known to exist in this material [17,18]. Subsequent DFT studies [13–15] have further scrutinized the influence of the stacking on the electronic structure. Reference [15] showed that the lowest energy structure exhibits a specific stacking of bilayers, dubbed "$AL$" stacking (with $A$ referring to the center of the SOD and $L$ to the upper right corner). These DFT results suggest that hybridization gaps, i.e., bonding-antibonding splittings originating from the strong inter-layer hopping within bilayers, make the low-temperature phase of 1$T$-$TaS_2$ band insulating. While this picture may be appropriate for the bulk, and does not rely on Mott physics, in a weakly correlated system, a metallic surface state would appear when the cleavage occurs within a bilayer. This is at odds with recent STM measurements [8,9] observing a gapped surface spectral function for both the cleavage plane within and between bilayers. A single-particle picture is thus not capable of consistently explaining the experimental findings, which calls for a systematic study of the correlated electronic structure in stacked bilayer systems.

In this Letter, we employ the $GW$ + extended dynamical mean field theory ($GW$ + EDMFT) method [19–22] to simulate semi-infinite systems of 1$T$-$TaS_2$ layers with the bilayer stacking identified in Refs. [8,9,15] and for the two different surface terminations. In the absence of on-site and

 

inter-site interactions, our model calculations produce a metallic surface state for the termination within the bilayer, but this state undergoes a Mott transition if realistic interactions are added. Our results are in good agreement with previously published STM and our own spatially resolved photoemission data, and clarify the interplay between gaps induced by intrabilayer hybridization and those arising from electronic correlations in the CCDW phase of $1T$-$TaS_2$.

*Model and method.*—The effective noninteracting single-band Hamiltonian $\mathcal{H}_{\mathrm{Ta}}$ for the SOD clusters of the $1T$-$TaS_2$ monolayer was obtained with density functional theory (DFT) as described in Ref. [23] and the Supplemental Material (SM) [24]. Our goal here is to model a system consisting of a semi-infinite sequence of bilayers with AL stacking and the two different surface terminations, as illustrated by the sketches in Fig. 1. For this, we explicitly construct a Hamiltonian $\mathcal{H}_{ab}$ for eight layers, labeled by letters $a, b = 1, \ldots, 8$, and periodically repeat the solution for layers 7 and 8 to mimic an infinite bulk. The AL stacking configuration features bilayers in which the SOD centers are aligned in the $c$ direction, whereas a shift of $-2\mathbf{a}$ is present between two neighboring bilayers (stacking vector $\mathbf{T}_S = -2\mathbf{a} + 2\mathbf{c}$, with $\mathbf{a}$, $\mathbf{b}$, $\mathbf{c}$ denoting the primitive vectors of the unit cell). We will denote the setup with cleavage plane between bilayers as "$A$ termination," and the setup with the cleavage plane within a bilayer as "$L$ termination." Several *ab inito* studies emphasized that the overlap between the $d_{z^2}$-like effective orbitals results in strong interplane hopping within a bilayer, while the hybridizations between bilayers are weaker. In order to build $\mathcal{H}_{ab}$ we introduce two off-diagonal hopping parameters $t^A_{ab}$ and $t^L_{ab}$ connecting, respectively, nearest-neighbor layers forming a bilayer and shifted layers:

$$\mathcal{H}_{ab}(\mathbf{R}_i, \mathbf{R}_j) = \mathcal{H}_{\mathrm{Ta}}(\mathbf{R}_i, \mathbf{R}_j)\delta_{ab} - t^A_{ab}\delta_{\mathbf{R}_i,\mathbf{R}_j} - t^L_{ab}(\mathbf{R}_i, \mathbf{R}_j), \tag{1}$$

where $\mathbf{R}_i \equiv \{\mathbf{R}_x, \mathbf{R}_y\}_i$ are the vectors of the unit cell. The Fourier transform of $t^A_{ab}$ has no component in the $\{\mathbf{k}_x, \mathbf{k}_y\} \equiv \mathbf{k}_\parallel$ plane. After a $-2\mathbf{a}$ translation, a cluster orbital has three neighbors in the adjacent layer, one in the same unit cell and two in neighboring unit cells, leading to an off-diagonal or $\mathbf{k}_\parallel$-dependent hybridization. While the distances to the different unit cells are not identical, given their small difference, we connect the three unit cells with the same $t^L_{ab}$. The $GW$ + EDMFT method [20–22,28–33] employed to study the effect of electronic correlations is similar to the real-space extension which has recently been applied to compounds with several sites in the unit cell [22,31,32] (see SM). To each layer, we associate an EDMFT-type impurity problem with fermionic and bosonic Weiss fields, which is solved using a continuous-time Monte Carlo method capable of dealing with retarded interactions [34–37]. These solutions provide a set of local self-energies $\Sigma^{\mathrm{EDMFT}}_{aa}(i\omega_n)$ and polarizations $\Pi^{\mathrm{EDMFT}}_{aaaa}(i\Omega_n)$ which replace the corresponding components of the local projection of their $GW$ counterparts (calculated for an eight-atom supercell and $20 \times 20$ $\mathbf{k}_\parallel$ points). The result is a momentum-dependent self-energy $\Sigma_{ab}(\mathbf{k}_\parallel, i\omega_n)$ and polarization $\Pi_{adbc}(\mathbf{k}_\parallel, i\Omega_n)$ which incorporates the effects of strong local and weaker nonlocal interactions. In the last step of the $GW$ + EDMFT self-consistency loop $\Sigma_{ab}(\mathbf{k}_\parallel, i\omega_n)$ and $\Pi_{adbc}(\mathbf{k}_\parallel, i\Omega_n)$ are used to compute the lattice Green's function $G_{ab}(\mathbf{k}_\parallel, i\omega_n)$ and screened interaction $W_{adbc}(\mathbf{k}_\parallel, i\Omega_n)$ [24]. Given the insulating nature of the material, we assume a Coulomb-like bare interaction which depends on the spatial coordinates as

$$U_{aabb}(\mathbf{R}_i, \mathbf{R}_j) = U\delta_{ab}\delta_{\mathbf{R}_i,\mathbf{R}_j} + \frac{V}{|\mathbf{R}_i - \mathbf{R}_j + \mathbf{r}_a - \mathbf{r}_b|}, \tag{2}$$

where $U$ is the local Hubbard interaction and $V$ a parameter that sets the strength of the nonlocal density-density interactions responsible for the screening of the effective on-site interaction [38], and $\mathbf{r}_a$ the position of the cluster orbital along the $c$ axis. With $\mathcal{H}_{ab}(\mathbf{k}_\parallel)$ and $U_{aabb}(\mathbf{k}_\parallel)$ as input, the $GW$ + EDMFT scheme provides a self-consistent solution

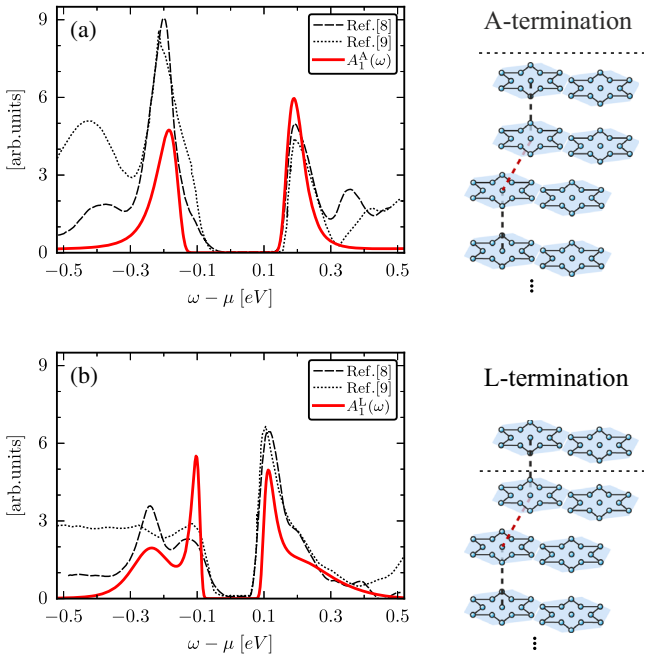


FIG. 1. Comparison between the $\mathbf{k}_\parallel$-integrated spectral function (red line) of the surface layer and the recent STM measurements of Refs. [8,9] (black lines) for the $A$ (a) and $L$ (b) termination. In the right column we sketch the cleavage planes which result in the two types of terminations. Black and red dashed lines indicate, respectively, the vertical hoppings $t^A_{ab}$ and $t^L_{ab}$ within the supercell.

where the effective local interaction $\mathcal{U}(\omega)$ on a given cluster site is screened by nonlocal charge fluctuations.

To capture the effect of the semi-infinite bulk, we add an embedding potential $E(\mathbf{k}_\parallel, i\omega_n)$ to the eighth layer. $E$ is computed with a continued fraction recursive formula that periodizes the properties of the last two layers:

$$E(\mathbf{k}_\parallel, i\omega_n) = \cfrac{t_{67}^2}{z_7 - \cfrac{t_{78}^2}{z_8 - \cfrac{t_{67}^2}{z_{7-\ldots}}}}, \tag{3}$$

where $t_{ab}^2 = \mathcal{H}_{ab}(\mathbf{k}_\parallel)\mathcal{H}_{ba}^*(\mathbf{k}_\parallel)$, with $ab \in \{67, 78\}$, and $z_a = i\omega_n + \mu - \mathcal{H}_{\mathrm{Ta}}(\mathbf{k}_\parallel) - \Sigma_{aa}(\mathbf{k}_\parallel, i\omega_n)$ with $a \in \{7, 8\}$. As we will see below, eight layers are enough to reach the bulk behavior, where the self-energy becomes layer independent. All calculations are performed at half-filling, i.e., with eight electrons in the supercell, and at a temperature of 30 K.

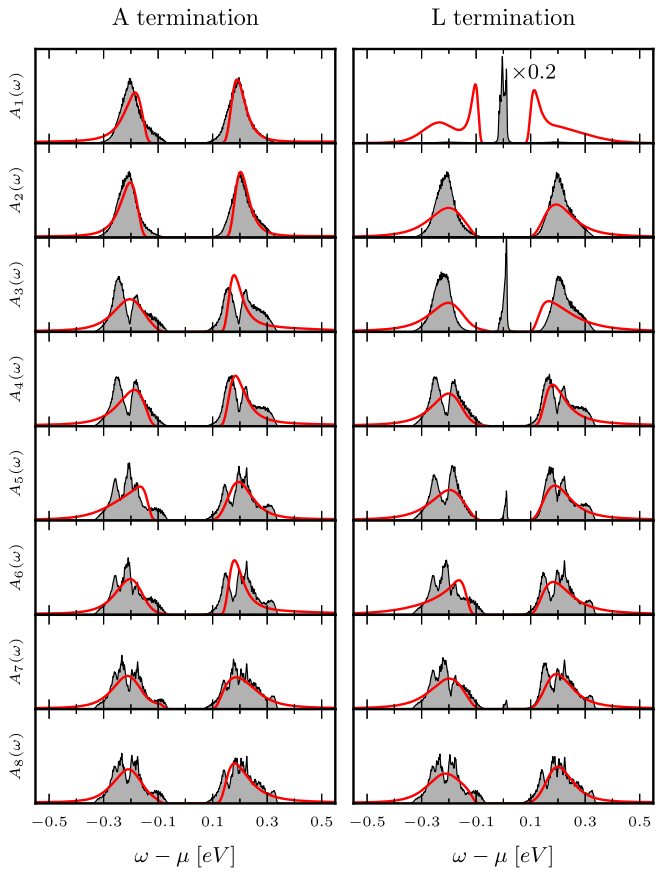


FIG. 2. Layer resolved $\mathbf{k}_\parallel$-integrated spectral function for the setup with $A$ termination (left) and $L$ termination (right). The $GW$ + EDMFT results (red lines) are superimposed to gray regions indicating the spectral functions of the noninteracting model. Without interactions, the model with $L$ termination hosts a metallic state pinned to the surface and decaying inside the structure. This surface state undergoes a Mott transition if the interactions are included. The noninteracting spectrum of the surface layer with $L$ termination has been scaled with a factor 0.2 for graphical purposes. The appearance of the metallic peaks on odd layers reflects the two-atom unit cell.

*Results.*—Our model of the layered structure depends on four parameters: the hoppings in the vertical direction $t_{ab}^A$ and $t_{ab}^L$, the local Hubbard interaction $U$, and the magnitude of the nonlocal density-density interaction $V$. To determine these parameters we first applied $GW$ + EDMFT to the $1T$-$TaS_2$ monolayer for which STM measurements are available and show a gap $\Delta \sim 0.4$ eV [39]. A good agreement with the STM spectra of Ref. [39] is obtained for $U = 0.4$ eV and $V = 0.08$ eV [33]. The values of $t_{ab}^{A,L}$ were subsequently determined by reproducing the STM measurements reported in two recent studies [8,9] on the surface effects of stacking ordering in $1T$-$TaS_2$. This yields $t_{ab}^A = 0.2$ eV and $t_{ab}^L = 0.045$ eV. The above set of Hamiltonian parameters allows to reproduce the main features of the experimental spectra, as shown in Fig. 1, which plots in black the recent STM measurements and in red the theoretical $\mathbf{k}_\parallel$-integrated surface spectral function $A_1^{A,L}(\omega)$. In particular, for both setups one obtains a good match for the gap size, with $\Delta_1^A \sim 0.4$ eV ($\Delta_1^L \sim 0.22$ eV) in the system with $A$ ($L$) termination. In the case of $L$ termination, also the higher-energy spectral features look consistent with the experimental data. STM features beyond $\pm 0.4$ eV most likely originate from bands which are not contained in our low energy model.

The layer-resolved spectral functions are reported in Fig. 2, where one notices that, already at the noninteracting level (gray regions), our model produces qualitatively different results for the two terminations. In the case of the $A$ termination, where no bilayers are broken, the system is a band insulator, which suggests that even in the presence of sizable interactions, the insulating character is primarily due to bonding-antibonding splittings. In contrast, the uncorrelated setup with $L$ termination hosts a metallic state at the surface, which extends only a few layers into the bulk. It is worth noticing that the embedding potential prevents the appearance of a surface state at the bottom of the eight-layer structure. The metallic peak in the layer-resolved densities of states disappears everywhere when the interactions are included, with a clear splitting of the peak of the surface layer into lower and upper Hubbard bands. This shows that the insulating nature of the system with $L$ termination is, in the surface region, the result of Mott physics. In the SM we provide further evidence of the correlation-driven insulating state in the surface layer by plotting the imaginary part of the EDMFT self-energies. $\mathrm{Im}\Sigma_{aa}^{\mathrm{EDMFT}}(i\omega_n)$ is very small and vanishes for $\omega_n \to 0$ in all the layers except for the surface layer with $L$ termination, where the low-frequency behavior shows a divergence as one expects for a paramagnetic Mott insulator. Hence, the insulating nature of the system with $L$ termination results from a combination of band-insulating and Mott insulating behavior. While the bulk of perfectly stacked $1T$-$TaS_2$ is a band insulator with a hybridization gap induced by the strong $t^A$ hopping within the bilayers,

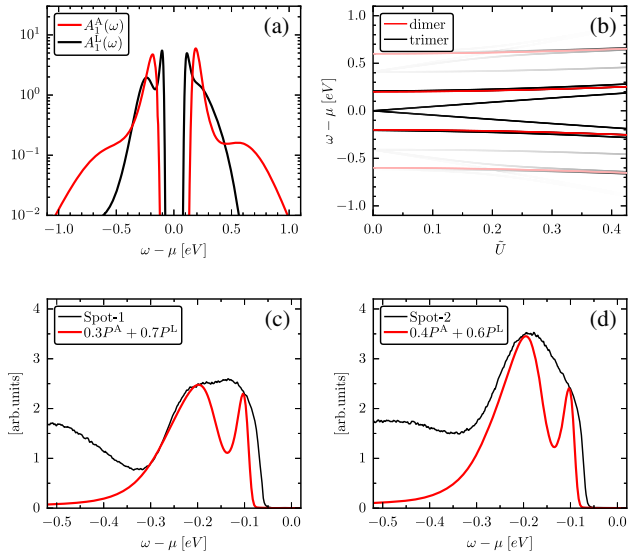


FIG. 3. The log-plot in panel (a) magnifies the high energy features of the $\mathbf{k}_\parallel$-integrated spectral function of the surface layer for the two terminations. Red (black) lines in panel (b) indicate the excitation energies of the Hubbard dimer (trimer) as a function of the local interaction $\tilde{U}$, where the color intensity indicates the $\tilde{U}$-dependent weight of the different excitations. Black lines in panels (c) and (d) show the experimental PES profiles obtained in different regions of a $1T$-$TaS_2$ sample, while red lines indicate the theoretical PES signals averaged over the two terminations as described in the text. The peak widths in the theoretical spectra are controlled by the parameters of the analytical continuation procedure.

the top layer of the system with $L$ termination, or an unpaired layer within a bulk with stacking disorder, behaves like a Mott insulating mono-layer of $1T$-$TaS_2$.

To clarify the nature of the peaks in the surface-layer spectra $A_1^{A,L}(\omega)$ we solved a two-site Hubbard model (dimer) with an intersite hopping $t = 0.2$ eV and a three-site Hubbard model (trimer) with $t_{12} = 0.045$ eV and $t_{23} = 0.2$ eV. To label the Hamiltonian blocks we considered only the charge quantum number and computed, as a function of the on-site repulsion $\tilde{U}$, the ground states with $N = 2$ and 3, respectively, plus the eigenenergies of the two adjacent charge sectors $N \pm 1$. The single-particle excitation energies with respect to the Fermi level $\pm(E_n^{N\pm1} - E_0^N)$ of the dimer (trimer) are shown by the red (black) lines in Fig. 3(b). The line width is indicative of the relative weight of the pole in the local spectrum $-(1/\pi)\mathrm{Im}G_a(\omega)$ (in the trimer case we considered the weakly hybridized site). In the dimer results, representative of the system with $A$ termination, one notices that the spectrum is gapped even at $\tilde{U} = 0$, while an increase of the local interaction splits the poles further. These observations are in agreement with the noninteracting spectra of Fig. 2. The red poles closest to the Fermi level correspond to electron and hole excitations to bonding-antibonding states, $|\psi_0^{N=3}\rangle = (1/\sqrt{2})(|\uparrow\downarrow,s\rangle - |s,\uparrow\downarrow\rangle)$ and $|\psi_0^{N=1}\rangle = (1/\sqrt{2})\times(|0,s\rangle + |s,0\rangle)$, where $s = \uparrow$ and $s = \downarrow$ are degenerate. The trimer model has an additional pole at zero frequency, which is split by the interaction into two excitation energies that, for relevant values of $\tilde{U}$, remain separated from the bonding-antibonding states at higher energies. While the $\tilde{U}$ parameters of the simple dimer and trimer models cannot be directly compared with the bare $U$ or effective $\mathcal{U}(\omega)$ interactions in the full calculation, for $\tilde{U}$ lower than the bare $GW$ + EDMFT interaction of $U = 0.4$ eV the dimer exhibits a larger gap than the trimer, which is consistent with the surface spectral functions reported on a log-scale in Fig. 3(a), and with our interpretation in terms of a bonding-antibonding and Mott gap. Furthermore, the high-energy poles of the two minimal models consistently explain the high-energy spectral weight obtained in the full calculations.

In agreement with several experimental observations [40–43], our spatially resolved photoemission spectroscopy (PES) data, shown in Fig. 3, indicate the presence of two substructures with a separation of about 0.1 eV close to the Fermi level. By performing a raster scan of the sample surface with a focused 6.2 eV laser source, we found that

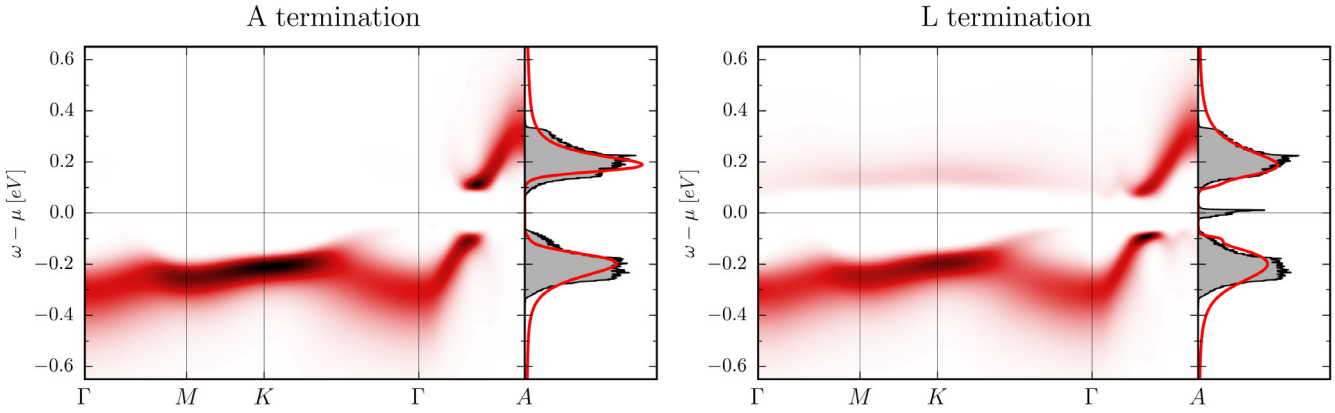


FIG. 4. Momentum-resolved spectral functions of the interacting system for the two types of terminations. The dispersion along the Γ-$A$ direction has been obtained by Fourier transforming the layer-resolved spectral function at each $\mathbf{k}$ point along the Γ-$M$-$K$-Γ path. Also indicated on the right are the local spectral functions for the noninteracting (gray) and interacting (red) model.

these substructures vary in relative intensity across the sample (see SM). Based on the different gaps obtained for the $A$ and $L$ termination, and the short penetration depth of photoemission, we argue that this observation is due to the superposition of PES signals from different spatial domains with the two types of terminations. Assuming that electrons contributing to the PES signal are emitted with a probability that decays exponentially from the surface of the sample, proportional to $\exp(-|z|/|\mathbf{c}|)$, the theoretical PES for the two terminations $P^{A,L}$ can be computed as a weighted average of the spectra over the layers, multiplied by the Fermi distribution for 30 K. The red lines in Figs. 3(c) and 3(d) show that different weighted averages allow to qualitatively explain the two substructure seen in the experimental spectra.

The insulating solution that we find for all layers when correlations are included implies that the electronic bands of the system are gapped also along the $c$ axis. Even though we do not have a periodic structure in the $c$ direction, we can nevertheless provide indications on how the dispersion along $\Gamma$-$A$ looks. We first interpolate the layer-resolved Green's function along a high-symmetry path within the planar Brillouin zone and then compute the Fourier transform along the $z$ direction as

$$G(\mathbf{k}_{\parallel}, \mathbf{k}_z, \tau) = \frac{1}{8}\sum_{ab} e^{i\mathbf{k}_z(\mathbf{z}_a - \mathbf{z}_b)} G_{ab}(\mathbf{k}_{\parallel}, \tau), \qquad (4)$$

where $\mathbf{k}_{\parallel} \in \{\Gamma - M - K - \Gamma\}$ and $\mathbf{k}_z \in \{\Gamma - A\}$. The maximum entropy method [44] is then used for the analytical continuation to the real-frequency axis. The result is shown in Fig. 4, while the momentum-resolved spectral functions for the different layers are reported in the SM. As expected, for both terminations we find a similar gap of the spectrum along the $\Gamma$-$A$ direction. The most notable difference is a weak and weakly dispersive band in the unoccupied part of the spectrum for the $L$ termination, the upper Hubbard band of the surface layer, which may be detectable with two-photon photoemission.

*Conclusions.*—We solved a minimal multilayer model to clarify how electronic correlations affect the bulk and surface states of $1T$-$TaS_2$ in the low-temperature CCDW phase. These calculations demonstrate that electronic correlations are responsible for the Mott insulating surface state in systems terminating with a broken bilayer, while the bulk layers are essentially band insulating. For appropriate interlayer hopping amplitudes, our approach reproduces with remarkable accuracy the spectra observed in recent STM measurements showing different gap sizes depending on the cleavage plane. We furthermore provide a natural explanation of the presented photoemission data in terms of a superposition of different spatial regions with $A$ and $L$ termination. In both cases we can interpret the high-energy ($\omega \approx \pm 0.4$ eV) substructures in the spectra as originating from a bonding-antibonding gap resulting from the strong intrabilayer hybridization, while the lower-energy peaks can be associated with the Mott insulating state pinned to the surface of the sample. Our results provide a solid basis for the previous interpretations of the STM measurements [8,9] and show that the surface region of $1T$-$TaS_2$ in the CCDW phase exhibits a nontrivial interplay between band insulating and Mott insulating behavior.

F. P., D. P., O. V. Y., and P. W. acknowledge support from the Swiss National Science Foundation through NCCR MARVEL. F. P. and P. W. acknowledge support from the European Research Council through ERC Consolidator Grant No. 724103. C. W. N., B. S., and C. M. acknowledge support from the Swiss National Science Foundation Grant No. P00P2_170597. The calculations were performed on the Beo05 clusters at the University of Fribourg and the Piz Daint cluster at the Swiss National Supercomputing Centre (CSCS) under projects ID mr26 and s1008.

[1] J. Wilson, F. D. Salvo, and S. Mahajan, Adv. Phys. **24**, 117 (1975).
[2] P. Fazekas and E. Tosatti, Philos. Mag. B **39**, 229 (1979).
[3] B. Sipos, A. F. Kusmartseva, A. Akrap, H. Berger, L. Forro, and E. Tutis, Nat. Mater. **7**, 960 (2008).
[4] M. Klanjsek, A. Zorko, R. Zitko, J. Mravlje, Z. Jaglicic, P. K. Biswas, P. Prelovsek, D. Mihailovic, and D. Arcon, Nat. Phys. **13**, 1130 (2017).
[5] L. Stojchevska, I. Vaskivskyi, T. Mertelj, P. Kusar, D. Svetin, S. Brazovskii, and D. Mihailovic, Science **344**, 177 (2014).
[6] D. Cho, S. Cheon, K.-S. Kim, S.-H. Lee, Y.-H. Cho, S.-W. Cheong, and H. W. Yeom, Nat. Commun. **7**, 10453 (2016).
[7] I. Vaskivskyi, I. A. Mihailovic, S. Brazovskii, J. Gospodaric, T. Mertelj, D. Svetin, P. Sutar, and D. Mihailovic, Nat. Commun. **7**, 11442 (2016).
[8] C. J. Butler, M. Yoshida, T. Hanaguri, and Y. Iwasa, Nat. Commun. **11**, 2477 (2020).
[9] J. Lee, K.-H. Jin, and H. W. Yeom, Phys. Rev. Lett. **126**, 196405 (2021).
[10] Z. Wu, K. Bu, W. Zhang, Y. Fei, Y. Zheng, J. Gao, X. Luo, Z. Liu, Y.-P. Sun, and Y. Yin, Phys. Rev. B **105**, 035109 (2022).
[11] Y. A. Gerasimenko, P. Karpov, I. Vaskivskyi, S. Brazovskii, and D. Mihailovic, npj Quantum Mater. **4**, 32 (2019).
[12] P. Darancet, A. J. Millis, and C. A. Marianetti, Phys. Rev. B **90**, 045134 (2014).
[13] T. Ritschel, J. Trinckauf, K. Koepernik, B. Büchner, M. v. Zimmermann, H. Berger, Y. I. Joe, P. Abbamonte, and J. Geck, Nat. Phys. **11**, 328 (2015).
[14] T. Ritschel, H. Berger, and J. Geck, Phys. Rev. B **98**, 195134 (2018).
[15] S.-H. Lee, J. S. Goh, and D. Cho, Phys. Rev. Lett. **122**, 106404 (2019).
[16] D. Shin, N. Tancogne-Dejean, J. Zhang, M. S. Okyay, A. Rubio, and N. Park, Phys. Rev. Lett. **126**, 196406 (2021).
[17] K. Fung, J. Steeds, and J. Eades, Physica (Amsterdam) **99B+C**, 47 (1980).
[18] K. Nakanishi and H. Shiba, J. Phys. Soc. Jpn. **53**, 1103 (1984).

[19] S. Biermann, F. Aryasetiawan, and A. Georges, Phys. Rev. Lett. **90**, 086402 (2003).
[20] T. Ayral, S. Biermann, and P. Werner, Phys. Rev. B **87**, 125149 (2013).
[21] F. Nilsson, L. Boehnke, P. Werner, and F. Aryasetiawan, Phys. Rev. Mater. **1**, 043803 (2017).
[22] F. Petocchi, V. Christiansson, and P. Werner, Phys. Rev. B **104**, 195146 (2021).
[23] D. Pasquier and O. V. Yazyev, Phys. Rev. B **105**, L081106 (2022).
[24] See Supplemental Material at http://link.aps.org/supplemental/10.1103/PhysRevLett.129.016402 for a detailed description of the real-space implementation, which includes Refs. [25–27].
[25] P. Giannozzi, S. Baroni, N. Bonini, M. Calandra, R. Car, C. Cavazzoni, D. Ceresoli, G. L. Chiarotti, M. Cococcioni, I. Dabo *et al.*, J. Phys. Condens. Matter **21**, 395502 (2009).
[26] J. P. Perdew, K. Burke, and M. Ernzerhof, Phys. Rev. Lett. **77**, 3865 (1996).
[27] A. A. Mostofi, J. R. Yates, Y.-S. Lee, I. Souza, D. Vanderbilt, and N. Marzari, Comput. Phys. Commun. **178**, 685 (2008).
[28] P. Werner and M. Casula, J. Phys. Condens. Matter **28**, 383001 (2016).
[29] L. Boehnke, F. Nilsson, F. Aryasetiawan, and P. Werner, Phys. Rev. B **94**, 201106(R) (2016).
[30] T. Ayral, S. Biermann, P. Werner, and L. Boehnke, Phys. Rev. B **95**, 245130 (2017).
[31] F. Petocchi, F. Nilsson, F. Aryasetiawan, and P. Werner, Phys. Rev. Research **2**, 013191 (2020).
[32] F. Petocchi, V. Christiansson, F. Nilsson, F. Aryasetiawan, and P. Werner, Phys. Rev. X **10**, 041047 (2020).
[33] J. Chen, F. Petocchi, and P. Werner, Phys. Rev. B **105**, 085102 (2022).
[34] P. Sun and G. Kotliar, Phys. Rev. B **66**, 085120 (2002).
[35] P. Werner, A. Comanac, L. de' Medici, M. Troyer, and A. J. Millis, Phys. Rev. Lett. **97**, 076405 (2006).
[36] P. Werner and A. J. Millis, Phys. Rev. Lett. **104**, 146401 (2010).
[37] H. Hafermann, P. Werner, and E. Gull, Comput. Phys. Commun. **184**, 1280 (2013).
[38] Since all the layers turn out to be insulating, screening is not very relevant and we expect the qualitatively same results even without nonlocal interactions.
[39] H. Lin, W. Huang, K. Zhao, S. Qiao, Z. Liu, J. Wu, X. Chen, and S.-H. Ji, Nano Res. **13**, 133 (2020).
[40] L. Perfetti, P. A. Loukakos, M. Lisowski, U. Bovensiepen, H. Berger, S. Biermann, P. S. Cornaglia, A. Georges, and M. Wolf, Phys. Rev. Lett. **97**, 067402 (2006).
[41] M. Ligges, I. Avigo, D. Golež, H. U. R. Strand, Y. Beyazit, K. Hanff, F. Diekmann, L. Stojchevska, M. Kalläne, P. Zhou, K. Rossnagel, M. Eckstein, P. Werner, and U. Bovensiepen, Phys. Rev. Lett. **120**, 166401 (2018).
[42] L. Perfetti, P. A. Loukakos, M. Lisowski, U. Bovensiepen, M. Wolf, H. Berger, S. Biermann, and A. Georges, New J. Phys. **10**, 053019 (2008).
[43] I. Avigo, P. Zhou, M. Kalläne, K. Rossnagel, U. Bovensiepen, and M. Ligges Phys. Rev. Lett. **120**, 166401 (2019).
[44] M. Jarrell and J. Gubernatis, Phys. Rep. **269**, 133 (1996).